Quantitative Analysis of the Effects of Intrathylakoid pH and Xanthophyll Cycle Pigments on Chlorophyll *a* Fluorescence Lifetime Distributions and Intensity in Thylakoids†

Adam M. Gilmore,‡ Vladimir P. Shinkarev,§ Theodore L. Hazlett,|| and Govindjee*,§

Photobioenergetics Group, Australian National University Research School of Biological Sciences, Canberra, 0200 ACT, Australia, and Departments of Biochemistry and Plant Biology, Center for Biophysics and Computational Biology, and Laboratory for Fluorescence Dynamics, Physics Department, University of Illinois at Urbana−Champaign, Urbana, Illinois 61801

Received June 11, 1998; Revised Manuscript Received July 16, 1998

ABSTRACT: The xanthophyll cycle-dependent dissipation of excitation energy in higher plants is one of the most important regulatory and photoprotective mechanisms in photosynthesis. Using parallel time-resolved and pulse-amplitude modulation fluorometry, we studied the influence of the intrathylakoid pH and the xanthophyll cycle carotenoids on the PSII chlorophyll (Chl) *a* fluorescence yield in thylakoids of *Arabidopsis*, spinach, and barley. Increases in concentrations of dithiothreitol in thylakoids, which have a trans-thylakoid membrane pH gradient and are known to have decreased conversion of violaxanthin (V) to zeaxanthin (Z), lead to (1) decreases in the fractional intensity of the ∼0.5 ns Chl *a* fluorescence lifetime (τ) distribution component and simultaneous increases in a 1.6−1.8 ns fluorescence component and (2) increases in the maximal fluorescence intensity. These effects disappear when the pH gradient is eliminated by the addition of nigericin. To quantitatively explain these results, we present a new mathematical model that describes the simultaneous effects of the chloroplast trans-thylakoid membrane pH gradient and xanthophyll cycle pigments on the PSII Chl *a* fluorescence τ distributions and intensity. The model assumes that (1) there exists a specific binding site for Z (or antheraxanthin, A) among or in an inner antenna complex (primarily CP29), (2) this binding site is activated by a low intrathylakoid pH (pK ≈4.5) that increases the affinity for Z (or A), (3) about one Z or A molecule binds to the activated site, and (4) this binding effectively "switches" the fluorescence τ distribution of the PSII unit to a state with a decreased fluorescence τ and emission intensity (a "dimmer switch" concept). This binding is suggested to cause the formation of an exciton trap with a rapid intrinsic rate constant of heat dissipation. Statistical analysis of the data yields an equilibrium association constant, K_a, that ranges from 0.7 to 3.4 per PSII for the protonated/activated binding site for Z (or A). The model explains (1) the relative fraction of the ∼0.5 ns fluorescence component as a function of both Z and A concentration and intrathylakoid pH, (2) the dependence of the ratio of F'_m/F_m on the fraction of the 0.5 ns fluorescence τ component (where F'_m and F_m are maximal fluorescence intensities in the presence and the absence of a pH gradient), and (3) the dependence of the ratio of F'_m/F_m on the concentration of Z and A and the intrathylakoid pH.

Interest in the molecular mechanisms used by higher plants to adapt and acclimate to light levels in excess of that used in photosynthesis has recently increased. One possible photoprotective mechanism involves xanthophyll cycle-dependent thermal dissipation of excess absorbed light energy in the light-harvesting complexes of photosystem II (PSII) (*1*−*8*). Light harvesting in the PSII antenna and the xanthophyll cycle-dependent heat dissipation mechanism are related to the structure and organization of the PSII pigment−proteins. The PSII holochrome is composed of (a) the PSII core that includes chlorophyll proteins CP43 and CP47 and reaction center proteins D1, D2, and cytochrome b_{559}, (b) the minor inner antenna, labeled as CP24, CP26, and CP29, and (c) the major peripheral antenna complex that includes trimeric assemblies of the light-harvesting complex (LHC) IIb (*9*). The peripheral and inner antennae contain both chlorophylls (Chls) *a* and *b* while the core exclusively contains Chl *a* and lacks Chl *b*. Like the Chl *b*, the xanthophylls lutein and neoxanthin are also distributed almost exclusively in the peripheral/inner antenna complexes. In

† A.M.G. and G. were supported by a training grant (DOE 92ER20095) from the Triagency (DOE/NSF/USDA) Program and its extension (DBI 96-02240) from the NSF for Collaborative Research in Plant Biology. V.P.S. was supported by USDA Grant 94-37306-0343. A.M.G. thanks the Australian National University (ANU) Research School of Biological Sciences (RSBS) for a research fellowship. T.L.H. and the Laboratory for Fluorescence Dynamics at the University of Illinois were supported by NIH Grant RR03155. The writing of this work was completed when Govindjee was on sabbatical leave at RSBS, ANU, Canberra, supported by an ANU fellowship.

* To whom correspondence should be addressed: University of Illinois, 265 Morrill Hall, MC-116, 505 South Goodwin Ave., Urbana, IL 61801-3707. Fax: 217-244-7246. E-mail: gov@uiuc.edu.

‡ Photobioenergetics Group, ANU/RSBS.

§ Departments of Biochemistry and Plant Biology and Center for Biophysics and Computational Biology, UIUC.

|| Laboratory for Fluorescence Dynamics, Physics Department, UIUC.

S0006-2960(98)01384-1 CCC: $15.00
Published on Web 09/09/1998

contrast to lutein and neoxanthin, the PSII pool of xanthophyll cycle pigments violaxanthin (V), antheraxanthin (A), and zeaxanthin (Z) is preferentially located in the minor CP complexes (80%) relative to the peripheral LHCIIb (20%) (*10*). The PSII core is enriched in β-carotene and lacks most xanthophylls (*10*). The xanthophyll cycle-dependent heat dissipation mechanism functions independently of the LHCI-Ib level per PSII, as indicated by experiments with Chl *b* deficient and Chl *b*-less mutants of barley, and is therefore believed to be largely associated with the CP complexes of the inner PSII antenna or core (reviewed in ref *7*).

Exposure of plants to excess light not only leads to reduced photosynthesis but also leads to quenching of chlorophyll fluorescence (called nonphotochemical quenching, NPQ). The details of this quenching mechanism are under debate (*1*−*8*). Nevertheless, it is known that both ΔpH and the pigments of the xanthophyll cycle are involved in this process (reviewed in refs *1*, *4*, and *7*). Several qualitative models for the combined effects of ΔpH and the pigments of the xanthophyll cycle have been proposed earlier (see refs *1*, *4*, and *7*). Here, we report, compare, and analyze the effects of intrathylakoid ΔpH and xanthophyll cycle pigments on both the Chl *a* fluorescence lifetime distributions and the pulse-amplitude modulation (PAM) intensity profiles in thylakoids from four different plants, namely, spinach (*Spinacea oleracea* L.), wild-type (WT) variety and chlorophyll *b* deficient nuclear gene mutant *chlorina f104 (clof104)* barley (*Hordeum vulgare* L.), and *Arabidopsis thaliana* L. cv. Columbia. Fluorescence lifetime measurements provide direct information on the fluorescence quantum yield and, thus, on the rate constants of the decay of the excited state. On the other hand, it is easier to measure fluorescence intensity (*F*) by commercial pulse-amplitude modulation (PAM) fluorometers. However, the intensity alone cannot distinguish between changes in the absorption cross section and the fluorescence quantum yield. To explain the observed results, we present a new quantitative model that describes the cumulative effects of both the chloroplast intrathylakoid pH and the xanthophyll cycle pigments Z and A on the PSII Chl *a* fluorescence lifetime distributions and intensity.

[1] Abbreviations: A, antheraxanthin; c_x, fluorescence lifetime center corresponding to the maximal amplitude value of the fluorescence lifetime distribution component labeled as *x*; Chl, chlorophyll; CPX, chlorophyll binding protein of PSII with molecular mass *X*; Diuron (DCMU), 3-(3,4-dichlorophenyl)-1,1-dimethylurea; DTT, dithiothreitol; $F_{m(0)}$, maximal Chl *a* fluorescence intensity with all Q_A reduced in the beginning of the experiment; F_m, maximal Chl *a* fluorescence intensity with all Q_A reduced in the absence of the proton gradient but in the presence of zeaxanthin (or antheraxanthin); F'_m, maximal Chl *a* fluorescence intensity with all Q_A reduced in the presence of the proton gradient and of zeaxanthin (or antheraxanthin); F_o, fluorescence intensity when all Q_A is in the oxidized state; f_x, fractional intensity of a fluorescence lifetime distribution component labeled as *x*; K_a, association equilibrium constant for binding of Z or A; LHCIIb, main light-harvesting pigment−protein complex of PSII; NPQ, nonphotochemical quenching of Chl *a* fluorescence; PAM, pulse-amplitude modulation fluorometer; PFD, photon flux density; PSI, photosystem I; PSII, photosystem II; P680, reaction center Chl *a* molecule, primary electron donor of PSII; Q_A, primary quinone electron acceptor of PSII; V, violaxanthin; w_x, width at half-maximum of the fluorescence lifetime distribution component labeled as *x*; WT, wild type; Z, zeaxanthin; ΔpH, trans-thylakoid membrane proton gradient; τ_x, fluorescence lifetime of component *x*; $\langle\tau\rangle = f_x\tau_x$, average fluorescence lifetime in the absence of the trans-thylakoid membrane pH gradient; $\langle\tau'\rangle = \sum f_x\tau_x$, average fluorescence lifetime in the presence of the trans-thylakoid membrane pH gradient.

MATERIALS AND METHODS

Plant Material and Thylakoid Preparation. Fresh spinach (*S. oleracea*) leaves were obtained locally and stored for at least 12 h (dark, 4 °C) before thylakoid isolation. Wild-type (WT) (*H. vulgare* L. cv. Donaria) and nuclear gene mutant *chlorina f104 (clof104)* barley plants were grown in the greenhouse. Barley seeds were germinated on a heating pad in potting soil covered with a layer of vermiculite. Plants were watered twice daily and fertilized once with a 20 N:20 P:20 K fertilizer applied at a concentration of 473 ppm N. Natural light was supplemented with high-intensity discharge lamps; the minimum photon flux density (PFD) was 400 ± 100 μmol of photons m^{-2} s^{-1} and the photo period was 14 h of light and 10 h of dark. *A. thaliana* L. cv. Columbia plants were grown in a growth chamber with a PFD of 230 μmol of photons m^{-2} s^{-1}, a photo period of 11.5 h, and a relative humidity of 90%. Barley plants were harvested after 8−10 days, whereas *Arabidopsis* plants were harvested after 8−10 weeks of growth. Leaves were dark adapted for at least 12 h at room temperature, then cut at their base, wrapped in a wet paper towel, and chilled in the dark for 1−2 h in a bag of ice in a 4 °C refrigerator. All thylakoid isolation procedures were performed in a darkened cold room (7 °C) under dim green light using chilled wares. The leaves (8−10 g) were cut into 2−3 cm pieces and ground using two to three 1-s bursts in a Waring blender in 100 mL of a slushy grinding buffer containing 0.33 M dextrose, 50 mM $Na_2HPO_4{\cdot}7H_2O$, 50 mM KH_2PO_4, 25 mM KCl, 5 mM $MgCl_2$, 0.1% BSA, and 0.2% sodium ascorbate, pH 6.5. The brie was gently vacuum filtered through a 41 μm nylon filter (Spectra/Mesh). The filtrate was centrifuged for 10 min at 1500*g* in an SS-34 (Sorvall) rotor at 4 °C. The pellet was gently resuspended in buffer A containing 0.33 M sorbitol, 4 mM EDTA, 5 mM $MgCl_2$, 2 mM $MnCl_2$, 0.1 M HEPES, and 0.2% BSA, pH 7.6. The reaction mixture (buffer B) contained 0.1 M sucrose, 10 mM NaCl, 10 mM KCl, 5 mM $MgCl_2$, 10 mM Tricine, 1 mM KH_2PO_4, and 0.2% BSA, pH 8.0. The following ingredients were added to buffer B immediately prior to the experiments: 30 mM sodium ascorbate to mediate deepoxidation of violaxanthin to zeaxanthin, 50 μM methyl viologen to mediate linear electron transport, and 0.3 mM ATP to fuel ATP hydrolysis. We call this final reaction mixture buffer C. The Chl concentration was determined according to the equations of Porra et al. (*12*).

Fluorescence Measurements. Fluorescence lifetimes (τs) were measured by using a cross-correlation, multifrequency, phase and modulation fluorometer (ISS Inc., Champaign, IL). Samples were excited with 610 nm light from the output of a cavity-dumped rhodamine 6G dye laser (Coherent, Palo Alto, CA) synchronously pumped by a mode-locked Nd:YAG laser. Chl *a* fluorescence was observed at wavelengths longer than 620 nm through a Hoya R-64 long pass filter. A scattering solution of glycogen in distilled water was used as the lifetime reference (0 ns), and a Corion 610 nm interference filter was placed in the emission path to isolate the scattering signal. Excitation path and emission path polarizers were set at 0° and 55°, respectively, to eliminate polarization artifacts in the fluorescence decay measurements

(*13*). Phase and modulation data were collected at multiple modulation frequencies ranging from 7 to 300 MHz and were subsequently analyzed using Globals Unlimited analysis software (University of Illinois, Urbana, IL). Here, we accept that the Chl *a* fluorescence lifetimes of pigment−protein complexes are most realistically modeled assuming a distribution(s) of lifetimes (*14*−*18*), in accordance with the concepts of protein dynamics and conformational substates (*19*). Data were fit to a bimodal, Lorentzian lifetime distribution model. This model includes two components, c_1 and c_2, that are characterized by two lifetimes, τ_1 and τ_2, by full widths at half-maximum, w_1 and w_2, and by relative fractional intensities, f_1 and f_2 (where $f_1 + f_2 = 1.0$). Additional information on phase and modulation fluorometry and the use of lifetime distribution models can be found in the literature (*14*, *15*, *20*).

In addition to the lifetime of fluorescence measurements, changes in the Chl *a* fluorescence intensity were recorded with a pulse-amplitude modulation fluorometer (PAM 103, Heinz-Walz, Effeltrich, FRG). In all cases, both F_m and F'_m were obtained under conditions where the primary quinone electron acceptor of PSII, Q_A, was reduced to Q_A^- either by a 2 s pulse of white light PFD $\approx$ 10 000 μmol of photons m^{-2} s^{-1} (from a Schott model KL-1500 lamp, filtered through a Walz DT-Cyan infrared filter) or after the addition of 10 μM DCMU to the reaction mixture during a continuous exposure to white light (PFD = 500 μmol of photons m^{-2} s^{-1}).

Protocol for Xanthophyll Cycle-Dependent Nonphotochemical Quenching of Chl a Fluorescence. The protocol for our experiments involved the following eight steps. Step 1 was exposure of isolated thylakoid membranes to white light (PFD = 500 μmol of photons m^{-2} s^{-1}, passing through a Corning CS1-75 infrared filter) which led to the acidification of the intrathylakoid space (lumen). This acidification activated the deepoxidase (pH optimum, 5.2) that converted the diepoxide V to the monoepoxide A and to epoxide-free Z (*23*, *24*). The steady-state [Z] + [A] was further varied at this time and at this step by the addition of different, but still low, concentrations of the sulfhydryl reagent dithiothreitol (DTT) that specifically and quantitatively inhibited the deepoxidase (*25*) without inhibiting either the light-driven or ATPase-mediated proton pumps (*26*, *27*). In step 2, a high concentration (3 mM) of DTT was added for two purposes, first to stop further [Z] + [A] formation and second to ensure thiol activation of the chloroplast ATPase (*26*). Importantly, reversion of Z and A back to V did not occur in our system since exogenous NAD(P)H was not added to the reaction mixture to activate the zeaxanthin epoxidase enzyme (*28*). In step 3, the maximal steady-state fluorescence intensity, F'_m, was measured when the pH gradient was created by both light-driven electron transport and ATP hydrolysis. In step 4, diuron [3-(3,4-dichlorophenyl)-1,1-dimethylurea], an inhibitor of electron transport between the Q_A and the secondary quinone Q_B, was added to eliminate photochemical quenching of Chl *a* fluorescence by the oxidized primary quinone electron acceptor Q_A (*29*). Diuron also completely blocked the light-driven proton pump without inhibiting the ATPase proton pump (*26*). Methyl viologen, which was added prior to illumination in buffer C, was present to eliminate changes in the transfer of excitation energy from PSII to PSI (*26*, *30*). In step 5, chilling the reaction mixture to less than 5 °C slowed the ΔpH dissipation and allowed fluorescence measurements at steady-state pH conditions (*16*). In step 6, the steady-state fluorescence lifetimes (τ_fs) and F'_m were determined under conditions when the proton gradient was created by ATPase only. In step 7, the protonophoric uncoupler nigericin was used to dissipate the transmembrane proton gradient. In step 8, the fluorescence lifetimes (τ_fs) and intensities (F_m) were measured again. Xanthophyll cycle pigment analyses were done as described by Gilmore and Yamamoto (*31*).

pH Measurements. The intrathylakoid pH was measured using 9-aminoacridine as a probe (*32*). This method is suitable for measurements of pH gradient that is greater than 1.0 (*33*). The 9-aminoacridine fluorescence intensity was measured using a SLM-8100 spectrofluorometer (Spectronic Instruments, Champaign, IL) with excitation at 400 nm (4 nm slit) and emission monitored at 450 nm (4 nm slit). The 3 mL sample (15 °C) was illuminated, while being stirred, from the side using the PAM fiberoptics and light from a Schott KL-1500 microscope lamp, passed through both a Schott RG (>610 nm) and a Walz (infrared) DT cyan filter, resulting in a final PFD of 1600 μmol of photons m^{-2} s^{-1}. The reaction mixture was buffer B plus 50 μM methyl viologen and 0.3 mM ATP. Five millimolar DTT and 3 μM 9-aminoacridine were added prior to illumination, 10 μM DCMU was added after 5 min of illumination, and 2 μM nigericin was added after 10 min of illumination. Data were averaged for three independent thylakoid samples.

Iterative Model Fitting Routine. The best fitting pH values and the mean (±SD) relative equilibrium association constant K_a values (for [Z]/PSII and [A]/PSII) were determined using the iterative Solver routine in Excel 5.0 (Microsoft). The best fits were determined by maximizing the values of both the coefficient of determination (r^2) and an analysis of variance (F-test = one-tailed probability that the variations in the model were not significantly different from the variations in the data).

RESULTS

Using thylakoids from spinach, wild-type (WT) and *chlorina f104* barley, and *Arabidopsis*, we have reinvestigated the effects of the ΔpH (created by light and/or by ATPase) and the concentrations of Z and A (as varied by the addition of DTT) on the maximal chlorophyll *a* fluorescence intensities and lifetimes.

Effect of [DTT] on the Concentration of Antheraxanthin and Zeaxanthin. The violaxanthin deepoxidase catalyzes the conversion of violaxanthin (V) first to antheraxanthin (A) and then to zeaxanthin (Z). DTT is known to inhibit this deepoxidase (*25*). Figure 1A shows that addition of up to 0.4 mM DTT to wild-type (WT) barley thylakoids decreases the relative concentration of zeaxanthin (diamonds) by about 4-fold from a fractional value of about 0.4 to 0.1 of [V + Z + A]. In contrast to zeaxanthin, changes in the relative concentration of antheraxanthin (squares) are smaller; we observe a slight increase with a plateau at about 0.2 mM DTT. Then, there is a slight decrease of [A] at about 1 mM [DTT]. The sum of [Z] and [A] (circles) decreases with increasing [DTT]. Relative changes in [Z] and in [A] are shown when we plot the fraction of [Z] or [A] per total xanthophylls [V + Z + A] as a function of the fraction of

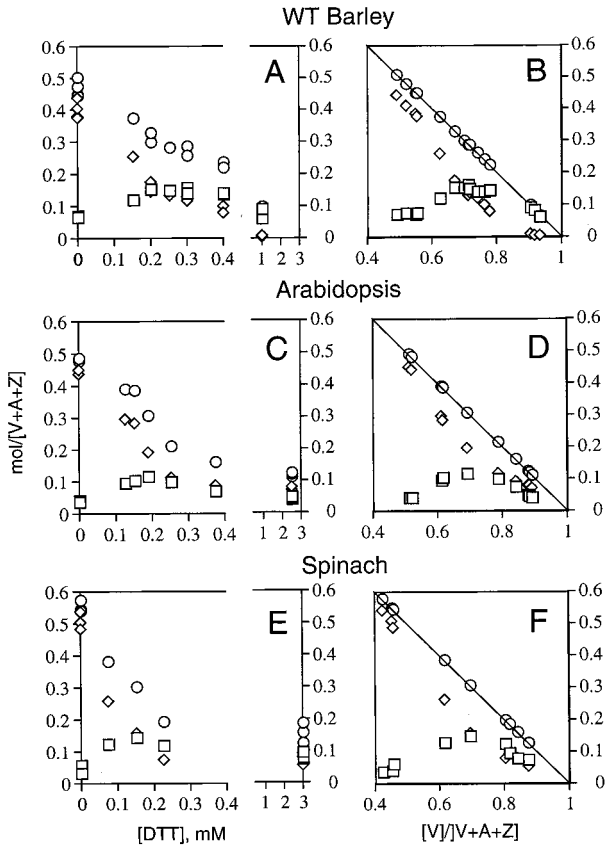

FIGURE 1: Dependence of the relative concentration of antheraxanthin (squares), zeaxanthin (diamonds), and Z + A (circles) on dithiothreitol (DTT) concentration (panels A, C, and E) and on the relative concentration of violaxanthin (panels B, D, and F) for thylakoids from WT barley, *Arabidopsis*, and spinach. Thylakoids were suspended, at 15 °C, in 3 mL of buffer C; [Chl *a* + *b*] was 15 μM. In all experiments, different concentrations of DTT were added prior to actinic illumination.

violaxanthin to the total xanthophylls (Figure 1B). At high (0.8−1 mM) violaxanthin concentrations, [A] decreases just as [Z] does. As expected, the fraction of [Z] + [A] decreases linearly with the fraction of V. Qualitatively, results similar to that in barley were obtained with *Arabidopsis* (panels C and D of Figure 1) and spinach (panels E and F of Figure 1), confirming the generality of the phenomenon under investigation.

pH Measurements. Using 9-aminoacridine fluorescence (*33*), we measured the intrathylakoid pH under three experimental conditions (pH gradient created by light, created by ATPase only, and dissipated by nigericin) in *Arabidopsis* (Figure 2A) and spinach (Figure 2B) thylakoids. The shaded bars show that the intrathylakoid pH is ∼4.5 under conditions when the pH gradient is created by light and is ∼5.3 when the pH gradient is created by ATP hydrolysis only. The largest value (about 8) was obtained when the pH gradient was dissipated with nigericin. We are aware that the value of the measurement in the pH 7−8 region, using 9-aminoacridine, is unreliable due to the lower sensitivity of the aminoacridine method at small values (<1.5) of the pH gradient (*33*). Since the intrathylakoid pH equilibrates with the reaction mixture (buffer B), which was measured to be pH 8 (hatched bar), the intrathylakoid pH must also be 8. Unshaded bars show the pH values predicted from a theoretical model (to be discussed later; see Discussion).

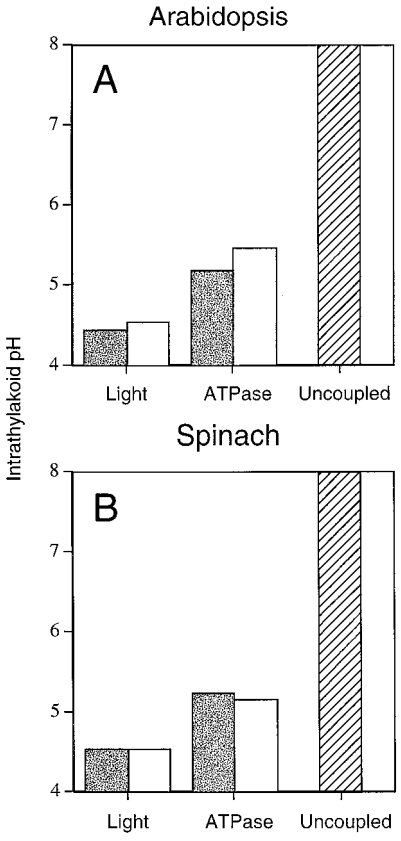

FIGURE 2: Intrathylakoid pH, measured by the 9-aminoacridine uptake (shaded bars), in *Arabidopsis* and spinach thylakoids under light-saturating (Light) and ATPase-mediated (ATPase) conditions. The hatched bar represents the pH of the uncoupled reaction mixture (buffer B). Unshaded bars show the results calculated from the theoretical model (see Discussion). The reaction mixture was buffer B plus 50 μM methyl viologen and 0.3 mM ATP. Five millimolar DTT and 3 μM 9-aminoacridine were added prior to illumination. Ten micromolar DCMU and 2 μM nigericin were added, respectively, after 5 and 10 min of illumination.

Results with spinach thylakoids were almost identical with those for *Arabidopsis*.

Effect of [DTT] on Nonphotochemical Quenching of Chlorophyll a Fluorescence. Here, we report the effects of the xanthophyll cycle pigment concentration (changed by the addition of DTT) on the pulse-amplitude modulation (PAM) chlorophyll a fluorescence intensity. Figure 3A shows a typical Chl *a* fluorescence intensity measurement for a spinach thylakoid suspension. The encircled numbers 1 through 8 refer to the steps in the experimental protocol (see Materials and Methods). After switching on a weak measuring light, we measured F_o (minimum fluorescence yield); then, after switching on a strong (actinic) light flash, we measured $F_{m(0)}$ (maximum fluorescence yield in the presence of a pH gradient but in the absence, we believe, of Z or A at the binding site). After switching on another strong, but continuous, light (see "On"), we observed first an increase and then a decrease in fluorescence (the Kautsky effect). After adding the same strong actinic light flash as before, we observed only small additional increases (see small spikes) in fluorescence yield. The difference between maxima of the spikes (called F'_m) and $F_{m(0)}$ is usually considered as a measure of nonphotochemical quenching. As shown in Figure 3A, after steps 2 (high DTT addition), 3 (measurement of F'_m), 4 (DCMU addition), and 5 (chilling),

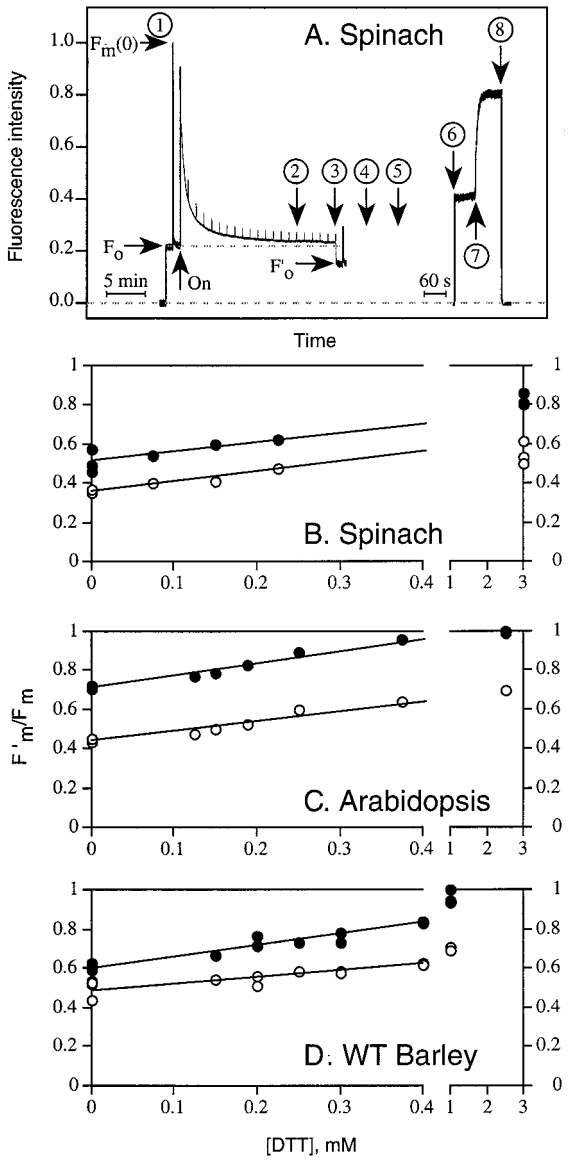

FIGURE 3: Effect of [DTT] on chlorophyll *a* fluorescence yields. Panel A shows the protocol of the experiment. The numbers refer to the steps of the protocol described in Materials and Methods. Panels B, C, and D show the dependence of F'_m/F_m (where F'_m and F_m are the maximum fluorescence yields obtained in the presence and the absence of the pH gradient) on [DTT] for thylakoids from spinach, *Arabidopsis*, and WT barley, respectively. Open circles (F'_m measured in step 3; F_m measured in step 8) represent data when the pH gradient was created by saturating light, whereas solid circles (F'_m measured in step 6; F_m measured in step 8) represent data when the pH gradient was created by ATPase only. Data shown here are from the same samples as those used in Figure 1. The reaction mixture was buffer B plus 50 μM methyl viologen and 0.3 mM ATP. Different concentrations of DTT were added prior to illumination. Ten micromolar DCMU and 2 μM nigericin were added at step 4 and step 7, respectively (see panel A).

a new F'_m was measured (step 6). Note that, after step 3, the strong continuous light was turned off, and a new F_o, called F'_o, was obtained. Then, in step 7, nigericin was added to measure F_m (maximum fluorescence yield in the absence of the pH gradient). For the case when the pH gradient was created by light, F'_m was measured after step 3 (i.e., before turning off the actinic light); for the case when the pH gradient was created by ATPase only, F'_m was measured at step 6. In the remainder of Figure 3, we plotted the influence of increasing concentrations of DTT (added at the very beginning of the experiment) on the ratio of maximal Chl *a* fluorescence intensity F'_m to F_m under either light-saturating (open circles, F'_m at step 3 divided by F_m at step 8) or ATPase-mediated (closed circles, F'_m at step 6 divided by F_m at step 8) conditions for intrathylakoid acidification in spinach (panel B), *Arabidopsis* (panel C), and WT barley (panel D) thylakoids. Although the nonphotochemical quenching (NPQ) has traditionally been plotted as $(F_m - F'_m)/F'_m$, we have plotted here the ratio of F'_m to F_m as a function of [DTT] because, as we will see later (Figure 4), this is linearly related to the concentration of bound zeaxanthin (Z) and antheraxanthin (A): increasing the concentration of bound Z and A decreases the F'_m/F_m. When the pH gradient is created either by light (bottom curves, open circles) or by ATPase (top curves, closed circles), F'_m/F_m increases with increasing [DTT] in all the three species. Generally, the influence of [DTT] on F'_m/F_m saturates above 1 mM DTT, which is consistent with the known inhibition of deepoxidation. Clearly, F'_m/F_m is significantly lower when the pH gradient is created by light than by ATPase. This difference is due to the higher ΔpH created by the light than by the ATPase (see Figure 2).

Figure 4 shows the dependence of F'_m/F_m, which characterizes nonphotochemical quenching of Chl *a* fluorescence, on the relative concentration of zeaxanthin (left panels), antheraxanthin (middle panels), and their sum (right panels) for barley (top panels), for *Arabidopsis* (middle horizontal panels), and for spinach (bottom panels) thylakoids. The quenching of Chl *a* fluorescence, as measured by F'_m/F_m, is stronger at higher [Z], whether the pH gradient was created by light (open circles) or by ATPase (closed circles). It is evident from this figure that the quenching of Chl *a* fluorescence is higher when the ΔpH is higher (created by light). This confirms the general view that both the pH gradient and the [Z] are important for the quenching of Chl *a* fluorescence. Panels B, E, and H show the dependence of F'_m/F_m on [A]. We observe that when [Z] is low (at high [DTT], see topmost points, both for open circles and for closed circles), increasing [A] increases the quenching of Chl *a* fluorescence (lowering of F'_m/F_m). This suggests A is a quencher of Chl *a* fluorescence under these conditions. However, when [Z] is significantly higher than [A], we observe a change in F'_m/F_m apparently in the opposite direction with increasing [A]; however, it should be realized that A converts directly to Z. The behavior of F'_m/F_m with increasing [Z] or [A] is explained by suggesting that the quenching of Chl *a* fluorescence depends on the sum of [A] and [Z]. This conclusion becomes obvious when we plot F'_m/F_m as a function of [Z + A] (see panels C, F, and I). Whether the pH gradient is created by light (open circles in each panel) or by ATPase (closed circles in each panel), the F'_m/F_m is found to decrease progressively with increasing [Z + A].

Concerted Effects of the Intrathylakoid pH and Xanthophyll Cycle Pigment Concentrations on the Chl a Fluorescence Lifetime Distributions. Figure 5 shows the Chl *a* fluorescence lifetime distributions in isolated thylakoid membranes of spinach (top panel) and wild-type (WT) barley (bottom panel) under the following conditions: (a) in the absence of nigericin, where a transmembrane pH gradient (ΔpH) is present (dashed curves), and (b) in the presence of

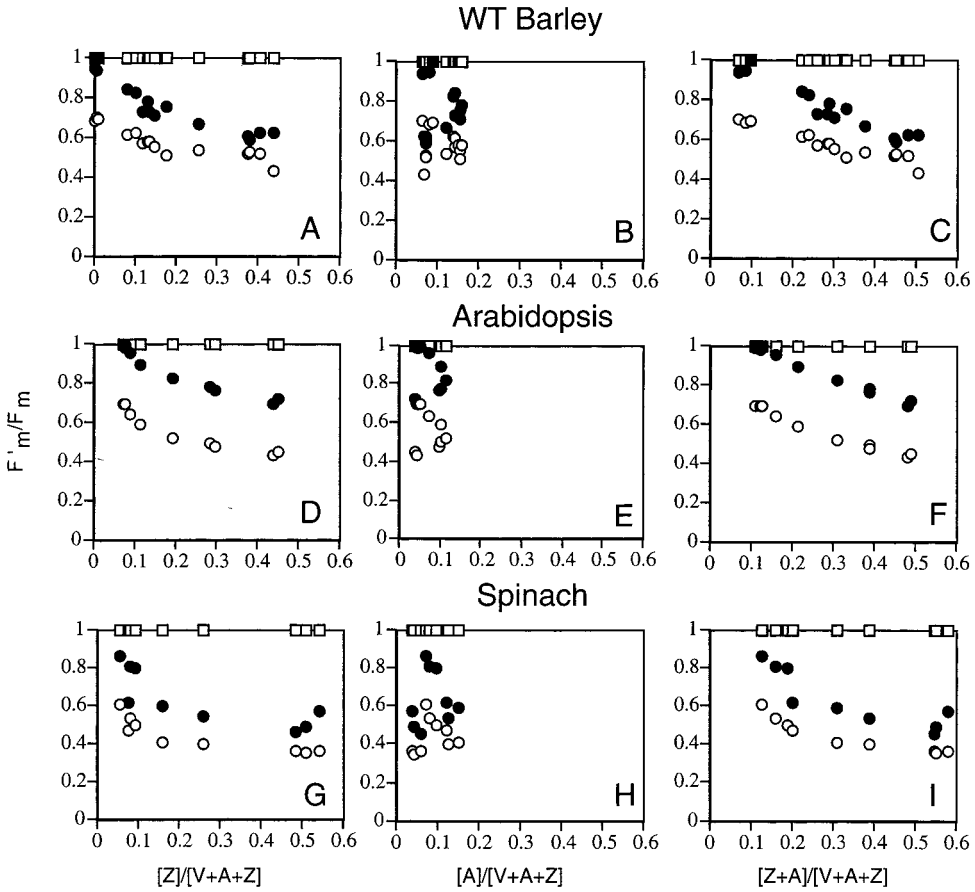

FIGURE 4: Dependence of F'_m/F_m (where F'_m and F_m are the maximum fluorescence yields obtained in the presence and the absence of the pH gradient) on the relative concentrations of zeaxanthin (Z, panels A, D, and G), antheraxanthin (A, panels B, E, and H), and Z + A (panels C, F, and I) in barley (panels A, B, and C), *Arabidopsis* (panels D, E, and F), and spinach (panels G, H, and I) thylakoids. Open circles represent data when the pH gradient was created by saturating light, solid circles represent data when the pH gradient was created by ATPase only, and squares represent data in the presence of nigericin. All other details are as described in the legend of Figure 3.

nigericin, where a ΔpH is absent (solid curves). In the experiments reported here, DTT was added first to decrease the [Z] and [A], and then nigericin was added. In the presence of a pH gradient, we observe two major components of fluorescence in both of the species. We refer to the long-lifetime component as c_1, its fractional intensity as f_1, and its lifetime center as τ_1, whereas the second short-lifetime component is referred to as c_2, its fractional intensity as f_2, and its lifetime center as τ_2. In spinach, for example, τ_1 is 1.8 ns and τ_2 is $\approx$ 0.46 ns. In the absence of DTT, the component c_1 has a low f_1, and the component c_2 has a high f_2. Decreasing [Z] + [A], by adding DTT, leads to decreases in the f_2 of the fluorescence lifetime distribution with the short-lifetime center ($\tau_2 \approx 0.46$ ns) and increases in the fractional intensity (f_1) of the long-lifetime center ($\tau_1 \approx 1.8$ ns). In barley, similar results were obtained. However, the barley τ_1 and τ_2 were 1.6 and 0.5 ns, respectively, and the width of the c_2 distribution was found to be wider (0.76 ns) than that of c_1 (0.5 ns).

In the presence of nigericin, when the trans-thylakoid pH gradient is absent (see solid curves), the Chl *a* fluorescence lifetime was not affected by changes in the [Z] and [A]. Here, the major distribution (with fraction f_1) is, however, centered at τ_1 of about 2.2 ns for spinach thylakoids and about 2.0 ns for barley thylakoids. It is clear that this component has shifted to slightly higher values from that before nigericin was added; further, the width of the lifetime distribution is wider in the absence of ΔpH than in its presence. Note, as shown in Table 1, that (a) these differences vary between spinach and barley and (b) in barley mutant *clof104*, which lacks most LHCIIb, these differences (*17*) in widths are much smaller than in the wild type. Thus, it is likely that the above-described differences in widths may also include effects on LHCIIb. These results are understood if we suggest that pH alone causes some conformational change in the vicinity of chlorophyll molecules in the pigment−protein complexes.

Table 1 contains the results of analysis of fluorescence data for thylakoids of spinach, WT barley, and barley mutant *clof104*, by assuming that there is a linear relationship between the fluorescence intensity ratio F'_m/F_m and the fractional intensity of the faster decaying fluorescence lifetime component c_2. All data for each species were linked to form a global data set. We note here that the fluorescence lifetime distribution center, width, and fractional intensity parameters were very similar to those reported earlier (*16*−*18*). The most significant difference noted between the earlier and this global-linked data set was an approximate 0.1 ns change in the lifetime values for each species. We note that the linear relationship between F'_m/F_m and f_2 was very similar between the WT barley and the barley mutant *clof104*, with both being slightly different from those for spinach. The intercept value in spinach was lower (∼20%) than in either the barley WT or *clof104*.

It is clear from a comparison of these results on the lifetime of Chl *a* fluorescence (Figure 5 and Table 1) with those on

Table 1: Resolved Global Parameters[a] from Analysis of Fluorescence Lifetime Data Constrained by Linking f_2, the Short-Lifetime Fractional Intensity, to the Observed Maximal Fluorescence Intensity with a Linear Model[b]

	Linking Equation: $f_2 = \text{Slope} \times (F'_m/F_m) + \text{Intercept}$					
	slope (p)	τ_1 (ns) (w_1 (ns))	intercept (p)	τ_2 (ns) (w_2 (ns))	r^2	χ^2
spinach	−1.1658 (≤0.001)	1.819 (0.397)	1.1549 (≤0.001)	0.456 (0.305)	0.9999	2.578
WT	−1.2557 (≤0.001)	1.629 (0.509)	1.4234 (≤0.001)	0.495 (0.756)	0.9999	0.862
clof104	−1.2506 (≤0.001)	1.588 (0.820)	1.4515 (≤0.001)	0.587 (0.943)	0.9999	0.523

[a] All phase and modulation data fits (phase error = 1°; modulation error = 0.020) were constrained to a bimodal Lorentzian distribution model where the distribution centers (τ_x) and widths (ω_x) were linked across all data files. For each thylakoid source, the fractional intensity (f_x) was linked through the linear equation and subsequently analyzed for the best fit to the lifetime data resolving both the lifetime parameters and the linking equation parameters. [b] The resolved lifetime, slope, and intercept values are reported from fluorescence studies of thylakoids from spinach ($n = 9$), wild-type barley (WT, $n = 15$), and the *chlorina f104* mutant of barley (*clof104*, $n = 13$). See Gilmore et al. (*16*, *17*) for a full summary of the unlinked fluorescence lifetime parameters and statistical analysis of the fluorescence lifetime data. The p values denote the probability for the null hypothesis of the slope or the intercept; r^2 is the coefficient of determination; n is the number of samples.

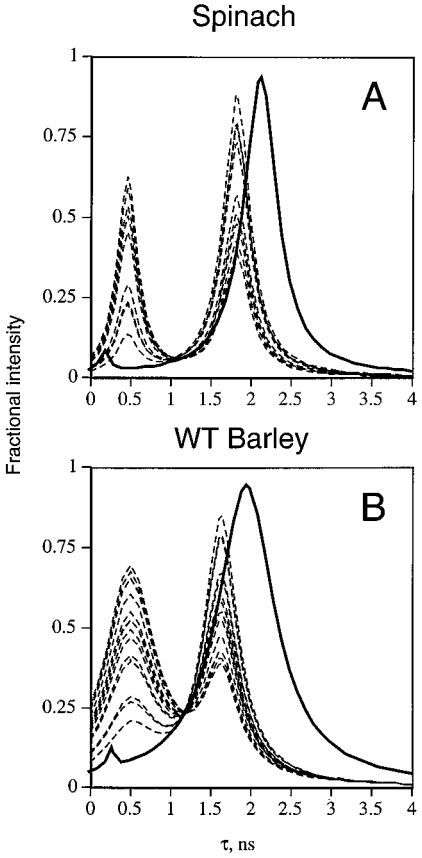

FIGURE 5: Fluorescence lifetime distributions of chlorophyll *a* in thylakoids from spinach (panel A) and WT barley (panel B). Dashed lines represent the chlorophyll *a* fluorescence lifetime distributions, measured at different dithiothreitol (DTT) concentrations (that changed the amounts of Z + A), under conditions when the pH gradient was created by ATP hydrolysis. Note that the short (0.5 ns) lifetime of the fluorescence component was found to decrease with increasing [DTT]. Solid lines represent the chlorophyll *a* fluorescence lifetime distribution, measured under the condition when the pH gradient was dissipated by 2 μM nigericin; the same curves were obtained at different [DTT]. Three milliliters of reaction mixture in all cases contained buffer C, thylakoids (7.5 μM Chl *a* + *b*), and 10 μM DCMU.

fluorescence intensities (Figure 3) that, at high [DTT] (low [Z + A]), high F'_m/F_m (low nonphotochemical quenching) is correlated with the presence of a smaller fraction (f_2) of the ~0.5 ns lifetime component and a higher fraction (f_1) of the ~2 ns lifetime component. On the other hand, at low [DTT] (high [Z + A]), low F'_m/F_m (high nonphotochemical quenching) is correlated with the presence of a higher fraction (f_2) of the 0.5 ns lifetime component and a lower fraction (f_1) of the 2 ns lifetime component. Thus, the presence of the fast component (c_2) with a lifetime of fluorescence of about 0.5 ns is correlated with the presence of Z. Figure 6 shows the dependence of the fraction f_2 of the component c_2 on the concentration of Z (panels A and D), of A (panels B and E), and of Z + A (panels C and F) in spinach (panels A, B, and C) and barley WT (panels D, E, and F) thylakoids. Data in panels A and D are suggestive of a saturation behavior of f_2 with increasing concentrations of Z; the same result is observed in panels C and F for Z + A. This suggests the presence of a limited number of binding sites for Z or A. It appears that the short lifetime component c_2 is due to the binding of the fluorescence quencher(s) Z and A.

Correlation between Chl a Fluorescence Lifetime and Intensity Measurements. Figure 7 (closed symbols) shows the correlation between the Chl *a* fluorescence lifetime and amplitude measurements for spinach (panels A, C, and E) and barley WT (B, D, and F) when the pH gradient was created by ATPase only. Fluorescence intensities, measured by PAM, are reported as both F'_m/F_m (panel A for spinach and panel B for WT barley) and the commonly used "nonphotochemical quenching" coefficient (or NPQ) $(F_m - F'_m)/F'_m$ (panels C and E for spinach and panels D and F for barley). Panels A and B plot f_2 as a function of F'_m/F_m; f_2 is a linear function of F'_m/F_m (see also Table 1). Panels C and D are plots of the fraction of the 0.5 ns component (f_2 values) against $(F_m - F'_m)/F'_m$ (equivalent to $F_m/F'_m - 1$ in the figure), obtained when ΔpH was induced by the addition of ATP; this dependence is, however, curvilinear. Panels E and F are for plots of $(\langle\tau\rangle'/\langle\tau\rangle) - 1$ as a function of $(F_m - F'_m)/F'_m$ values, where $\langle\tau\rangle'$ and $\langle\tau\rangle$ are the approximated average lifetimes of Chl *a* fluorescence $[\langle\tau\rangle = f_1\tau_1 + f_2\tau_2]$ at F'_m and F_m, respectively. Although the $\langle\tau\rangle$ and $\langle\tau\rangle'$ parameters do not account for differences in the distribution width or shape that can substantially alter the integrated average lifetime, they still serve in these linked analyses as quantitative predictors of the average lifetimes and of F_m and F'_m. Clearly, an almost linear relationship between these fluorescence lifetime and intensity parameters is observed. The observed relationships in panels A (and B) and E (and F) allow us to predict the lifetime of Chl *a* fluorescence and the fractions of the fast component (f_2) from fluorescence intensities (F'_m/F_m) measured by PAM. As an example of the application of this idea, we calculated values (see Table 1 and the legend of Figure 7 for details) for f_2 and for $(\langle\tau\rangle'/\langle\tau\rangle) - 1$ from F'_m and F_m measurements, under conditions when ΔpH was created by light (see open symbols in Figure

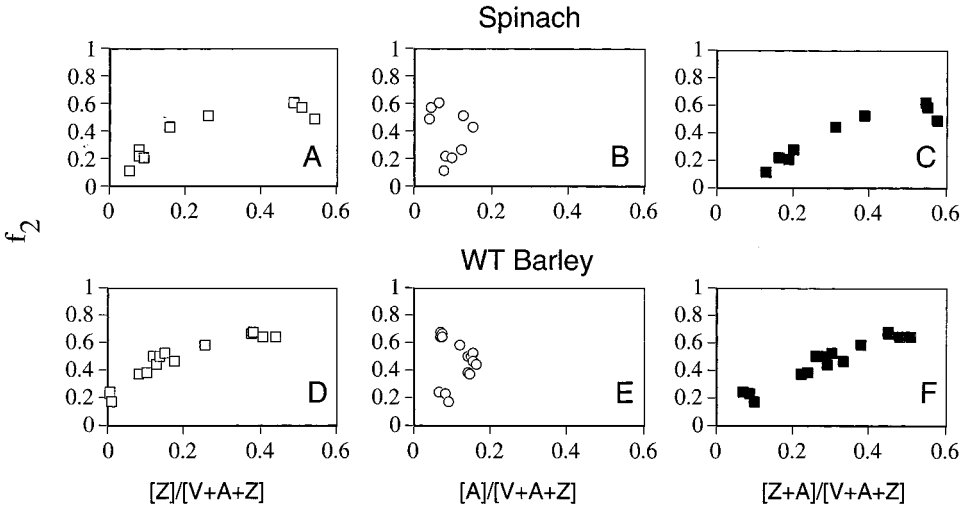

FIGURE 6: Relationship between the fractional intensity, f_2, of the c_2 lifetime component (~0.5 ns) and the xanthophyll cycle pigments zeaxanthin (Z, open squares), antheraxanthin (A, open circles), and their sum (Z + A, closed squares) in spinach (panels A, B, and C) and WT barley (panels D, E, and F) thylakoids.

7). Since f_2 is linearly related to F'_m/F_m, which decreases in proportion to increasing [Z + A] and decreasing intrathylakoid pH, changes in F'_m/F_m can be used as a direct monitor of the fluorescence lifetimes, intrathylakoid pH, and [Z + A].

DISCUSSION

Xanthophyll Cycle Quenching Scheme. Several qualitative models for the combined effects of ΔpH and the pigments of the xanthophyll cycle are available in the literature (see, e.g., refs *1*, *4*, and *7*). The effects of both the xanthophyll cycle pigments and ΔpH on the Chl *a* fluorescence lifetimes and intensities, obtained in this paper, can be explained by a scheme shown in Figure 8. According to this scheme, light-induced electron transport or ATPase acidifies the intrathylakoid space. This acidification (see Figure 2), which can be reversed by uncouplers, has a dual synergistic role. First (see bottom middle of Figure 8), it activates the violaxanthin deepoxidase, with a p*K* of about 5.2, converting violaxanthin (V) to antheraxanthin (A) and then to zeaxanthin (Z) (*34*), and second (see top middle of Figure 8), it leads to protonation of some carboxyl groups, with a p*K* of about 4.5, of the inner core of PSII, perhaps in CP26 and CP29 antenna complexes (*9*, *35*, *36*). Härtel et al. (*37*) showed that CP24 expression lags that of CP29 and of NPQ in the greening process of barley and therefore CP24 may not be necessary for induction of the major NPQ component. Further, Pesaresi et al. (*38*) have recently shown that a single point mutation on the glutamate residue 166 to glutamine (E166Q) in CP29 prevents binding of dicyclohexylcarbodiimide to this complex in vitro. Hence, it is most likely that this is the protonatable glutamyl residue that is directly involved in the protonation steps required for induction of xanthophyll cycle-dependent energy dissipation. This protonation of the CP(s) is suggested to cause an activation of a binding site for either Z or A, possibly via some conformational changes. The binding of Z or A is then suggested to cause a switching of PSII units to a state with an increased rate constant of heat dissipation (*16*−*18*), leading to the quenching of Chl *a* fluorescence (a "dimmer switch" effect), as measured by the pulse amplitude modulation fluorometer (Figures 3 and 4) or by multifrequency phase fluorometry (Figures 5 and 6). We note that the sulfhydryl reagent dithiothreitol (DTT) inhibits deepoxidation (*34*) without inhibiting either the light-driven or ATPase-mediated proton pumps. By varying the concentration of DTT, we were able to obtain different concentrations of Z and A (see Figure 1). Further, the uncouplers do not alter the [Z + A] in isolated thylakoid membranes unless NAD(P)H is added to activate the epoxidase enzyme (see refs *28* and *39*).

Kinetic Model for the Analysis of the pH and Xanthophyll Cycle Concentration Dependence of PSII Fluorescence. In the current model, only Z and A are considered as quenchers, although in other systems (e.g., *Chlamydomonas*), other molecules (e.g., lutein; see ref *40*) may also be considered without affecting the kinetic model presented here. Although a large number of Z and A molecules may be present in the total xanthophyll pool, only one molecule per PSII is suggested, for simplicity, to be involved in the energy dissipation mechanism. In our model, only bound Z and A can quench Chl *a* fluorescence because (a) no evidence exists for collisional quenching in the present system, (b) the most likely mechanism of quenching is the electron-exchange Dexter mechanism (see ref *41*), and (c) only Z and A, not V, can quench Chl *a* fluorescence, suggesting a specific binding niche. In our concept, each Z and A molecule has a given average probability to fill the activated binding niche and quench Chl *a* fluorescence.

To quantitatively incorporate the effects of the pH on the xanthophyll cycle-dependent Chl *a* fluorescence quenching, we assume that protonation of carboxyl moieties on the lumenal side of the PSII inner core antenna proteins (primarily CP29) is necessary for the reversible activation of the binding site for Z (or A). Here we note that there may be several carboxyl moieties (perhaps more than four, assuming two for each CP26 and CP29 unit per PSII) involved in the pH activation for each binding site. As implied from the work in ref *38*, it may be only CP29 that may have to be considered further. But, we must keep other options open. We may envision a scenario where protonation of the carboxyl groups releases counterions (probably divalent), thus changing the charged properties of these functional

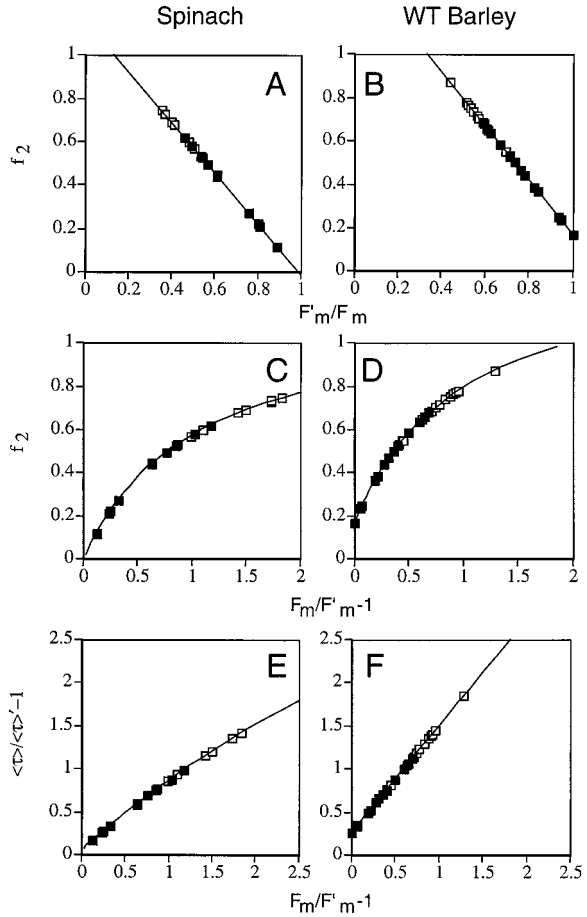

FIGURE 7: Correlation between chlorophyll *a* fluorescence lifetime and steady-state parameters in spinach (panels A, C, and E) and WT barley (panels B, D, and F) thylakoids. Panels A and B show the dependence of f_2 (fractional intensity of the 0.5 ns fluorescence component) on F'_m/F_m (where F'_m and F_m are the maximum fluorescence yields obtained in the presence and absence of the pH gradient). Panels C and D show the dependence of f_2 on nonphotochemical quenching $[(F_m - F'_m)/F'_m]$, and panels E and F show the dependence of $(\langle\tau\rangle - \langle\tau'\rangle)/\langle\tau'\rangle$ (where $\langle\tau'\rangle$ and $\langle\tau\rangle$ are the average lifetimes of chlorophyll *a* fluorescence in the presence and absence of the pH gradient) on nonphotochemical quenching $[(F_m - F'_m)/F'_m$, labeled as $F_m/F'_m - 1$ in the figure]. Closed symbols represent experimental data for samples when the pH gradient was made by ATPase; open symbols represent calculated data for samples when the pH gradient was made by light (for details, see text).

groups and hence their structural interaction with other neighboring functional amino acid groups, lipid headgroups, or proteins. We speculate that a dynamic refolding and/or rearrangement within and/or between CP proteins results in the exposure of the binding domain for Z and A.

To summarize the protonation step(s), we use the following simple scheme:

$$\underset{(W)}{H^+ + CP{-}COO^-} \overset{pK}{\rightleftharpoons} \underset{(X)}{CP{-}COOH} \qquad (1)$$

where W in parentheses denotes the binding site for Z and/or A and X denotes the protonated (activated) binding site that has a high binding affinity for Z (or A). We include both Z and A as quenchers of Chl *a* fluorescence, as discussed earlier under Results. The pH dependence of relative populations of these two states of the binding site is given by the Henderson−Hasselbach equation:

$$pH = pK + \log\frac{[W]}{[X]} \qquad (2)$$

We propose here that all the Z and A molecules present in the PSII unit compete for the binding site. For simplicity, we suggest that each molecule may bind with equal probability. A similar approach can be used even if Z and A had different binding efficiencies. The Z and A molecules interact in a reversible manner with this binding site. Therefore, the binding scheme in eq 3 is characterized by the equilibrium association constant K_a (here for simplicity we show only Z):

$$\underset{(X)}{Z + CP{-}COOH} \overset{K_a}{\rightleftharpoons} \underset{(Y)}{Z{-}CP{-}COOH} \qquad (3)$$

where Y in parentheses denotes the protonated (activated) binding site with Z present.

The equilibrium binding (association) constant K_a is given by the equation:

$$K_a = \frac{[Y]}{[X][Z]} \qquad (4)$$

Combining eqs 1 and 3 gives the reaction scheme:

$$\underset{(W)}{H^+ + CP{-}COO^-} \overset{pK}{\rightleftharpoons} Z + \underset{\substack{(X)\\(\tau_f = 1.6-2.0\ ns)}}{CP{-}COOH} \overset{K_a}{\rightleftharpoons} \underset{\substack{(Y)\\(\tau_f = 0.4-0.5\ ns)}}{Z{-}CP{-}COOH} \qquad (5)$$

The Chl *a* fluorescence lifetimes (τ_f) listed above are suggested ranges of values for the species (X and Y) in spinach. We note that the above-described protonation event, related to the activation of the binding site (see Figure 8), is not the same as that which leads to the change in lifetime of fluorescence from 2.2 to 1.8 ns (see Figure 7 for spinach). This may have a different origin, such as conformational changes.

Equations 2 and 4 together with the balanced equation for the binding site

$$[W] + [X] + [Y] = [Tot] \qquad (6)$$

yield the equation for the fraction of binding sites occupied by Z at steady state:

$$\frac{[Y]}{[Tot]} = \frac{[Y]}{[W] + [X] + [Y]} = \frac{[Z]K_a^{app}}{1 + [Z]K_a^{app}} \qquad (7)$$

where the apparent binding constant

$$K_a^{app} = \frac{K_a}{1 + 10^{pH-pK}} \qquad (8)$$

It is obvious from the right side of the eq 7 that the dependence of the fraction of occupied (Y) binding sites is described by a simple hyperbolic equation. On the other hand, the apparent binding constant (K_a^{app}) increases drastically as the pH falls below p*K* (eq 8).

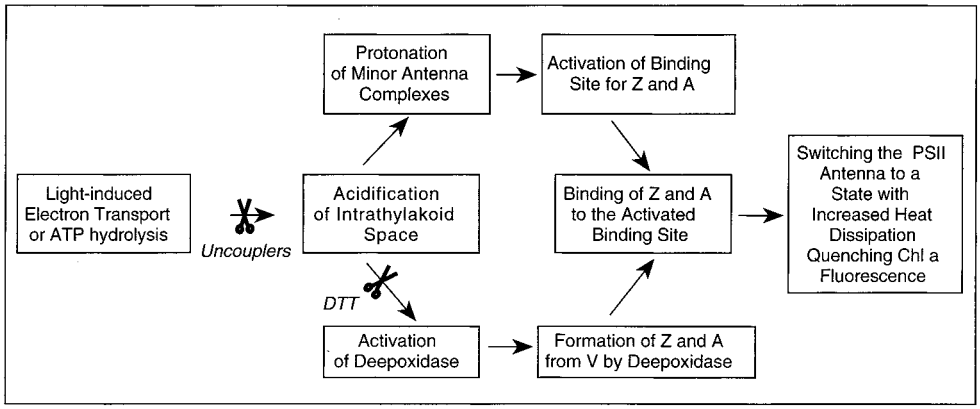

FIGURE 8: A model, consistent with our data, of how the intrathylakoid pH and xanthophyll cycle pigments lead to quenching of PSII chlorophyll *a* fluorescence yield (also, see refs *1*, *4*, and *7*).

Equation 7 can also be written using pK and K_a as

$$\frac{[Y]}{[Tot]} = \frac{K_a[Z]10^{pK-pH}}{1 + 10^{pK-pH}(1 + K_a[Z])} \quad (9)$$

We use eq 9 to analyze and fit our experimental data. We suggest that the introduced fractions (W), (X), and (Y) represent different states of the PSII units that have different respective fluorescent yields and lifetimes, as outlined in eq 5. We identify the fractions $[Y]/[Tot] = f_2$ and $[W + X]/[Tot] = f_1$ with the fractions of PSII units in the short ($\tau_f \approx 0.5$ ns) and long ($\tau_f \approx 1.9$ ns) Chl *a* fluorescence lifetime states, respectively. We emphasize that we have considered here the simplest case when only a single binding site for the quencher is present per PSII. If, however, there is more than one interacting binding site, eq 9 should be modified accordingly.

Relationship between the PSII Fractional Intensity, the Relative Zeaxanthin and Antheraxanthin Concentrations, and the Intrathylakoid pH. A major use of the model discussed above is in quantitatively explaining the combined data on the lifetime of the fluorescence, concentrations of the quenchers, and the intrathylakoid pH. The model allows us to analyze and discuss the pH and xanthophyll cycle-dependent changes in the PSII fluorescence yield with respect to pK and K_a values. Panels A−C of Figure 9 show plots of the fractional intensity of the 0.5 ns fluorescence component (f_2) against [Z] per PSII, under three intrathylakoid pH levels. The open squares represent the experimental points when the pH gradient is obtained by illuminating the samples with light, the closed squares when the pH gradient is obtained by the ATPase, and the closed circles when the pH gradient is dissipated by nigericin. Panels D−F of Figure 9 show plots of f_2 versus $[Z] + x[A]$ per PSII, where x is about 1, ranging from 0.83 to 1.34. For each pH condition in Figure 9 (panels D−F), the solid lines represent the model mean, while the dotted lines denote the (±) standard deviation range of the K_a values. The values of pH were taken from measurements with 9-aminoacridine (see Figure 2). The pK was assumed to be 4.5. Then, the experimental data points were fitted by eq 9 to find K_a. Panels G−I of Figure 9 show that when only [Z] is considered a quencher of fluorescence (open diamonds), then the calculated K_a values for each data point show large differences in all three types of materials; note especially that in Figure 9 (panel H, WT barley, and panel I, mutant barley *clof104*) there is a very large systematic deviation, reaching values of ∼100. Since K_a must be a constant for each sample point independent of the pH and $[Z + A]$, this result suggests that another parameter is needed to fit the curves correctly. As discussed earlier, [A] is also a possible quencher of Chl *a* fluorescence (see Figure 4). Thus, we fitted the experimental data points by using eq 9 but replacing [Z] with $[Z] + x[A]$ (see filled diamonds in Figure 9G−I). The newly calculated K_a values were found to fall in a narrow range. As shown in panels J−L of Figure 9, both the F-test and r^2 values for the model indicate that the best fitting relative value for the fraction of the total pool of $[A] = x$ is about equal to that of [Z], i.e., supporting the conclusion that A is a quencher (*42*) and $x \approx 1$.

Comparison of the Intrathylakoid pH Calculated from the Model to That Measured by Uptake of 9-Aminoacridine. In the above discussion, we had used the measured values of the pH gradient in calculating K_a. Now, we show below that even the value of pH can be estimated by fitting eq 9 with the experimental data. Figure 2 shows a comparison of these predictions (open bars) of the pH with those measured by 9-aminoacridine fluorescence quenching (shaded bars). The best fitting pH predictions were obtained by using the iterative fitting routine. The values from both the model and quenching of the 9-aminoacridine fluorescence yield closely parallel each other. The lowest intrathylakoid pH of ≈4.5 was measured under the light-saturating conditions (see "Light" in Figure 2), and the next lowest pH of ≈5.3 was obtained under the ATPase-mediated conditions (ATPase). Since there is no dependence of f_2 on $[Z + A]$ under uncoupled conditions, the model could not provide any insight here.

Biophysical and Photophysical Aspects Concerning the Roles of Antheraxanthin and Zeaxanthin. We can explain the quenching of Chl *a* fluorescence by Z and A, but not by V, by assuming that only Z and A can accept singlet excited-state energy from Chl *a* and subsequently dissipate this energy as heat (*8*, *41*). In this theory, the predicted energy level of violaxanthin is above, whereas that of antheraxanthin and zeaxanthin is below, that of the first excited singlet state of Chl *a*. The calculated lifetime of the singlet excited state of the carotenoid after accepting an exciton from Chl *a* is predicted to be $\tau = 9$ ps for zeaxanthin and $\tau = 14.4$ ps for antheraxanthin (*41*); however, this has not yet been measured.

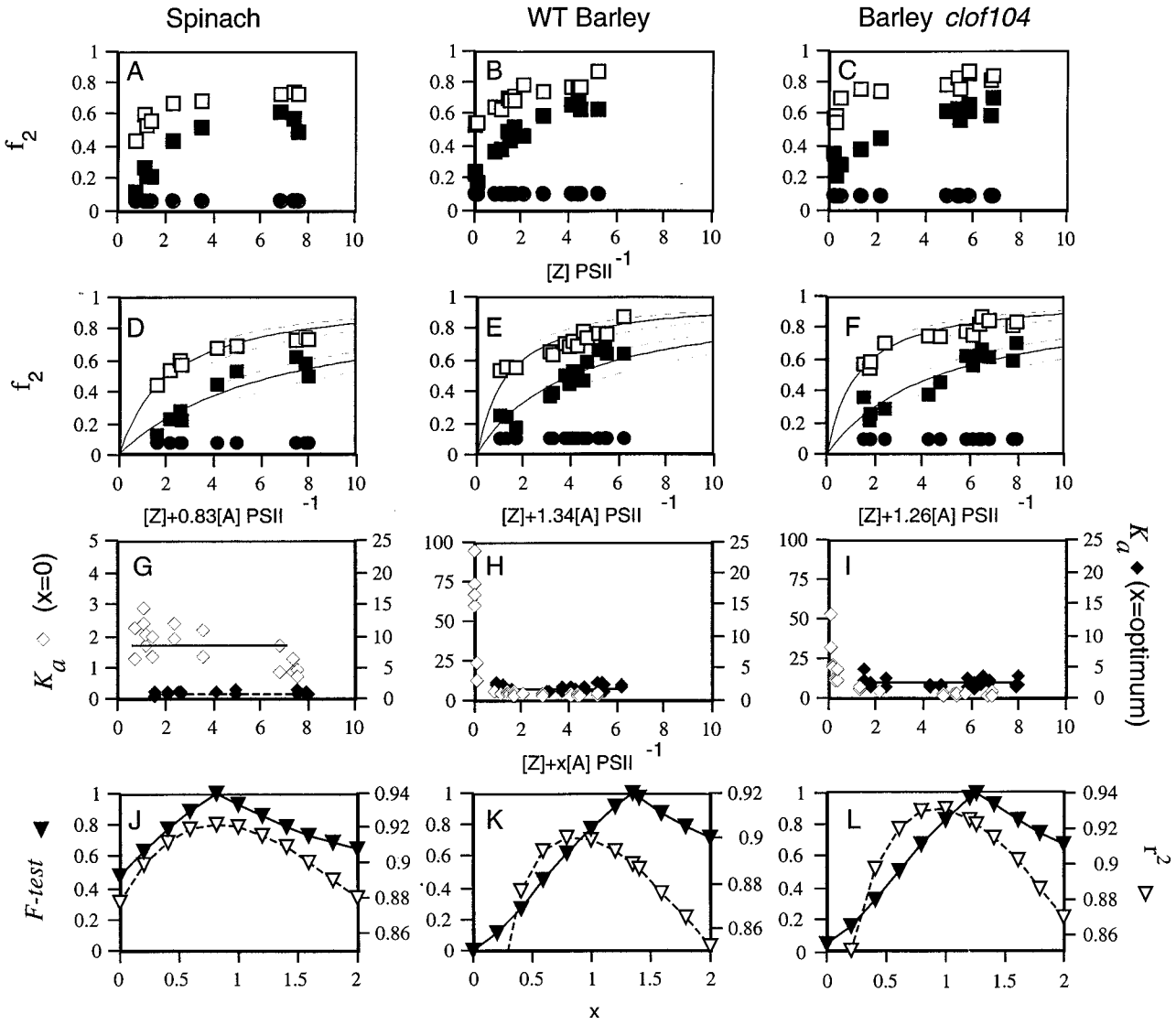

FIGURE 9: Top row: fractional intensity, f_2, of the 0.5 ns component as a function of the concentration of zeaxanthin (Z) per PSII under conditions when the pH gradient was made by light (open squares) or by ATPase (closed squares) and when the pH gradient was dissipated by nigericin (closed circles) in thylakoids from spinach, WT barley, and the barley mutant *clof104*. Second row: same as the first row except that f_2 is plotted as a function of [Z] + x[A]. Third row: association constant, K_a, as a function of [Z] + x[A] for $x = 0$ (open diamonds) and for x = optimal value (closed diamonds). Fourth row: the *F*-test and the r^2 for different values of x.

Frank et al. (*41*) have suggested a Dexter-based exchange mechanism which requires molecular orbital overlap and hence a very close physical proximity. We suggest that bound Z and A may indeed be in close proximity to Chls in the antenna complex; like the deepoxidation and epoxidation reactions (see ref *43*), this binding is probably stereospecific (*34*) for the Z and A and presumably facilitated by a pH-activated step (Figure 8). An alternate hypothesis to the idea of Frank et al. is that Z and A may trigger structural or conformational changes around Chl molecules in the vicinity of the binding site, indirectly increasing the internal conversion processes of the Chls and the entire PSII unit (*4*).

Concluding Remarks. Using parallel time-resolved and pulse-amplitude modulation (PAM) fluorometry, we have studied the influence of the intrathylakoid pH (measured by 9-aminoacridine uptake) and the xanthophyll cycle carotenoids (measured by HPLC) on PSII Chl *a* fluorescence yield in thylakoids of three different species. To quantitatively explain the combined effects of pH and of zeaxanthin plus antheraxanthin concentrations on time-resolved (Figures 5, 6, and 9) and steady-state (Figure 4) Chl *a* fluorescence, we have presented here a new quantitative model which assumes that (a) there exists a specific binding site for a few (for simplicity, one) zeaxanthin (or antheraxanthin) molecules among or in the inner antenna of PSII, (b) this binding site is activated by a low intrathylakoid pH that increases the affinity for zeaxanthin (or antheraxanthin), and (c) this binding effectively "switches" the fluorescence lifetime distribution of the PSII unit to a state with a decreased fluorescence lifetime and emission intensity (the idea of a dimmer switch). The model explains (a) changes in the relative fractional intensities of the ~0.5 ns fluorescence component as a function of both zeaxanthin (and antheraxanthin) concentration and intrathylakoid pH, (b) the dependence of the ratio of F'_m/F_m on the fraction of the 0.5 ns fluorescence lifetime component, and (c) the dependence of the ratio F'_m/F_m on both the concentration of zeaxanthin (and antheraxanthin) and intrathylakoid pH. Finally, and importantly (see Figures 7 and 9), the correlation between the measurements on the lifetime of fluorescence and amplitude,

statistically supported here for three higher plant species, allows one to predict the changes of [Z] both from the lifetime of fluorescence measurements and from the amplitude measurements with pulse amplitude fluorometers (PAM) that are available commercially.

ACKNOWLEDGMENT

We are indebted to Drs. Olle E. Björkman, Barbara Demmig-Adams, and William Adams III, their laboratory staff, and graduate students for the use of HPLC facilities and Ms. Purna Lakhia for her help in growing the plants and for laboratory assistance.

REFERENCES

1. Horton, P., Ruban A. V., and Walters, R. G. (1996) *Annu. Rev. Plant Physiol. Plant Mol. Biol. 47*, 655−684.
2. Björkman, O., and Demmig-Adams, B. (1994) *Ecol. Stud. 100*, 17−47.
3. Long, S. P., Humphries, S., and Falkowski, P. G. (1994) *Annu. Rev. Plant Physiol. Plant Mol. Biol. 45*, 633−662.
4. Demmig-Adams, B., Gilmore, A. M., and Adams, W. W., III (1996) *FASEB J. 10*, 403−412.
5. Demmig-Adams, B., and Adams, W. W., III (1996) *Trends Plant Sci. 1*, 21−26.
6. Yamamoto, H. Y., and Bassi, R. (1996) in *Oxygenic Photosynthesis: The Light Reactions* (Ort, D. R., and Yocum, C. F., Eds.) pp 539−563, Kluwer Academic Publishers, Dordrecht, The Netherlands.
7. Gilmore, A. M. (1997) *Physiol. Plant. 99*, 197−209.
8. Owens, T. G. (1996) in *Photosynthesis and the Environment* (Baker, N. R., Ed.) pp 1−23, Kluwer Academic Press, Dordrecht, The Netherlands.
9. Green, B. R., and Durnford, D. G. (1996) *Annu. Rev. Plant Physiol. Plant Mol. Biol. 47*, 685−714.
10. Bassi, R., Pineau, B., Dainese, P., and Marquardt, J. (1993) *Eur. J. Biochem. 212*, 297−303.
11. Horton, P., and Ruban, A. V. (1992) *Photosynth. Res. 34*, 375−385.
12. Porra, R. J., Thompson, W. A., and Kriedmann, P. E. (1989) *Biochim. Biophys. Acta 975*, 384−394.
13. Spencer, R. D., and Weber, G. (1970) *J. Chem. Phys. 52*, 1654−1663.
14. Jameson, D. M., and Hazlett, T. L. (1991) in *Biophysical and Biochemical Aspects of Fluorescence Spectroscopy* (Dewey, G., Ed.) pp 105−133, Plenum Press, New York.
15. Govindjee, Van de Ven, M., Cao, J., Royer, C., and Gratton, E. (1993) *Photochem. Photobiol. 58*, 438−445.
16. Gilmore, A. M., Hazlett, T. L., and Govindjee (1995) *Proc. Natl. Acad. Sci. U.S.A. 92*, 2273−2277.
17. Gilmore, A. M., Hazlett, T. L., Debrunner, P. G., and Govindjee (1996) *Photosynth. Res. 48*, 171−187.
18. Gilmore, A. M., Hazlett, T. L., Debrunner, P. G., and Govindjee (1996) *Photochem. Photobiol. 64*, 552−563.
19. Frauenfelder, H., Parak, F., and Young, R. D. (1988) *Annu. Rev. Biophys. Biophys. Chem. 17*, 451−479.
20. Gratton, E., Jameson, D. M., and Hall, R. D. (1984) *Annu. Rev. Biophys. Bioeng. 13*, 105−124.
21. Jahns, P., and Junge, W. (1990) *Eur. J. Biochem. 193*, 731−736.
22. James, D. R., Liu, Y.-S., Siemiarczuk, A., Wagner, B. D., and Ware, W. R. (1988) *Proc. SPIE−Int. Soc. Opt. Eng. 909*, 90−96.
23. Yamamoto, H. Y., Nakayama, T. O. M., and Chichester, C. O. (1962) *Arch. Biochem. Biophys. 97*, 168−173.
24. Hager, A. (1969) *Planta 89*, 224−243.
25. Yamamoto, H. Y., and Kamite, L. (1972) *Biochim. Biophys. Acta 267*, 538−543.
26. Gilmore, A. M., and Yamamoto, H. Y. (1992) *Proc. Natl. Acad. Sci. U.S.A. 89*, 1899−1903.
27. Sokolove, P. M., and Marsho, T. V. (1976) *Biochim. Biophys. Acta 430*, 321−326.
28. Siefermann, D., and Yamamoto, H. Y. (1975) *Arch. Biochem. Biophys. 171*, 70−77.
29. Duysens, L. N. M., and Sweers, H. E. (1963) in *Studies on Microalgae and Photosynthetic Bacteria* (Japanese Society of Plant Physiologists, Eds.) pp 353−372, University of Tokyo Press, Tokyo, Japan.
30. Horton, P., and Black, M. T. (1981) *Biochim. Biophys. Acta 635*, 53−62.
31. Gilmore, A. M., and Yamamoto, H. Y. (1991) *J. Chromatogr. 543*, 137−145.
32. Schuldiner, S., Rottenberg, H., and Avron, M. (1972) *Eur. J. Biochem. 25*, 64−70.
33. Pick, U., and McCarty, R. E. (1980) *Methods Enzymol. 69C*, 538−548.
34. Yamamoto, H. Y. (1979) *Pure Appl. Chem. 51*, 639−648.
35. Crofts, A. R., and Yerkes, C. T. (1994) *FEBS Lett. 352*, 265−270.
36. Walters, R. G., Ruban, A. V., and Horton, P. (1996) *Proc. Natl. Acad. Sci. U.S.A. 93*, 14204−14209.
37. Härtel, H., Lokstein, H., Grimm, B., and Rank, B. (1996) *Plant Physiol. 110*, 471−482.
38. Pesaresi, P., Sandona, D., Giuffra, E., and Bassi, R. (1997) *FEBS Lett. 402*, 151−156.
39. Gilmore, A. M., Mohanty, N., and Yamamoto, H. Y. (1994) *FEBS Lett. 350*, 271−274.
40. Niyogi, K. K., Björkman, O., and Grossman, A. R. (1997) *Proc. Natl. Acad. Sci. U.S.A. 94*, 14162−14167.
41. Frank, H. A., Cua, A., Chynwat, V., Young, A., Gosztola, D., and Wasielewski, M. R. (1994) *Photosynth. Res. 41*, 389−395.
42. Gilmore, A. M., and Yamamoto, H. Y. (1993) *Photosynth. Res. 35*, 67−78.
43. Bugos, R. C., Hieber, A. D., and Yamamoto, Y. (1998) *J. Biol. Chem. 273*, 15321−15324.

BI981384X